KSME

Springer

Journal of Mechanical Science and Technology 37 (12) 2023

Original Article
DOI 10.1007/s12206-023-1104-3

Keywords:
· Clearance fit
· Interference fit
· Spindle rotor-bearing system
· Vibration

Correspondence to:
Zinan Wang
wzn1404589743@126.com

Citation:
Wang, Z., Chen, S., He, W., Wang, Z., Xia, Z. (2023). Research for the bearing fit effect on the vibration characteristics of spindle rotor-bearing system. Journal of Mechanical Science and Technology 37 (12) (2023) 6257~6270.
http://doi.org/10.1007/s12206-023-1104-3

Received February 12th, 2023
Revised August 3rd, 2023
Accepted August 29th, 2023

† Recommended by Editor
No-cheol Park

Research for the bearing fit effect on the vibration characteristics of spindle rotor-bearing system

Zhan Wang, Siyang Chen, Wenzhi He, Zinan Wang and Zhongxian Xia

School of Mechanical Engineering, Shenyang Jianzhu University, Shenyang, China

Abstract Spindle bearing fits mainly include interference fit of inner ring and clearance fit of outer ring, which directly affect the vibration characteristics of spindle rotor-bearing system. In this paper, the influence of spindle bearing inner and outer ring fits on bearing support stiffness is firstly studied. Considering the spindle bearing inner and outer ring fits, a dynamic model of spindle rotor-bearing system is established. Then, the analysis methods of bifurcation and time domain are used to perform simulation analysis. The influence of bearing fit on the vibration characteristics of rotor system is researched. Lastly, at different rotating speeds, bearing fits experiments are conducted on built motorized spindle test platform, which verifies the correctness of the dynamic model. The results show that the influence of bearing fit on vibration is nonlinear. The influence of clearance fit on vibration is smaller, when the clearance fit value of bearing outer ring is about 4-6 μm. The vibration characteristics of rotor are more sensitive to the clearance fit of bearing outer ring than the interference fit of bearing inner ring. The research work provides an important theoretical basis for the optimal of spindle bearing assembly.

1. Introduction

In the aerospace, automotive and other industries, high precision CNC machine tools are used to process various equipment components. The motorized spindle is used as the core component of CNC machine tools. In order to facilitate its internal disassembly and improve interchangeability, the support bearing is usually mounted with different mating methods. This can affect the vibration characteristics of the spindle system [1]. Due to high speed operation of the spindle, the deformation for the bearing will increase the size of the inner and outer ring, changing the fit of the bearing installation. Therefore, the vibration and instability of the system may be increased [2]. It is important to study the effect of bearing fit changes on the dynamic characteristics of the rotor system. The optimal fit amount should be researched during the assembly process to reduce vibration. The ceramic bearing and the ceramic rotating shaft are connected by interference fit. Meanwhile, as the temperature of ceramic motorized spindle change, thermal displacement directly affects the interference fit. If the interference amount is becoming larger, the contact stress between the inner ring of the bearing and the shaft will be greater, which will aggravate the wear degree of the contact surface. If the interference amount is becoming smaller, the bearing will slip, which will increase the temperature caused by the sliding friction.

The spindle bearing fit usually includes the interference fit of inner ring and the clearance fit of outer ring. For the clearance fit, some scholars study its effect on the dynamic characteristics of the spindle system from the viewpoint of contact deformation [3] and collision [4]. Shi et al. [5, 6] presented a dynamic model of the clearance fit between full ceramic bearing and steel pedestal under large temperature range. It was found that selecting smaller clearance can reduce the influence of temperature on the dynamic behavior of the bearing outer ring. Wu et al. [7, 8] investigated the vibration response and dynamic force transmissibility of the rotor-bearing-

pedestal system under multiple clearances, then the increase of clearance will reduce the support stiffness and dynamic transmission efficiency. Mao et al. [9] analyzed the influence of roller bearing outer ring deformation on the dynamic characteristics of roller bearing, a small fit clearance has a positive effect on load distribution which was presented. Li et al. [10] analyzed the influence of bearing outer ring installed obliquely on the spindle thermal characteristics. It could conclude that inclined bearing outer ring can cause increased heat production. Wang et al. [11] demonstrated that squeeze film damper can effectively reduce the vibration of rotor system with the fit looseness fault between bearing outer ring and sleeve. Feng et al. [12] proposed a new equivalent mechanical analysis method to analyze the coupling problem of bearing clearance and support asymmetry.

In addition to the clearance fit of bearing outer ring, the interference fit of bearing inner ring affects the dynamic characteristics of rotor system. Some scholars have done some important work on this. Wang et al. [13] studied the effect of interference fit on the vibration of ceramic spindle system. The results of the paper is found that the bearing stiffness increase as the interference fit amount. Guo et al. [14] established the finite element model of machine tool spindle system considering the bearing interference fit. The bearing contact angle linearly decreases as the increase of interference fit values of bearing inner and outer rings. Gao et al. [15] also highlighted that the bearing interference fit can improve the spindle support stiffness and natural frequencies. It can be seen that there have been extensive researches into the bearing fit relationship in recent years. However, the existing literature has only studied the effects of the inner and outer ring fits on the system vibration separately, without considering both for analysis. Considering both inner and outer ring fits can produce more complex changes in the dynamic characteristics of the system, make the model more consistent with the actual motion of the spindle.

In this paper, inspired by the previous work, a dynamic model of spindle system with the clearance fit of outer ring and the interference fit of inner ring is proposed. The effects of bearing fit on the dynamic characteristics of the spindle are further investigated to seek the optimal fit to reduce the vibration. At different rotating speeds, bearing fits experiments are conducted on the motorized spindle test platform. The work lays a theoretical basis for further optimizing the assembly relationship and structural design of motorized spindle.

2. Dynamic modeling of spindle rotor-bearing system

The motorized spindle is a type of integrated electromechanical product that assembles the machine tool spindle and the motor into one unit. Its internal structure mainly consists of support bearings, stator, rotor and spindle, as shown in Fig. 1. Its power source is mainly an electric motor. Water cooling is adopted during operation, and cooling water channels are equipped outside the stator to achieve better heat dissipation. Oil and gas lubrication is utilized to ensure the stable operation of the system. In order to ensure that the motorized spindle owns better dynamic characteristics, the bearing inner ring and spindle adopt interference fit. Bearing outer ring adopts small clearance fit with bearing pedestal. The interference and clearance fits of bearing will lead to an extra elastic deformation of rotor and bearing parts, which have a great influence on the spindle dynamic characteristics.

2.1 Clearance fit model of bearing outer ring

The clearance fit of bearing outer ring is convenient for bearing installation and dismantlement. It can decrease the influence of bearing pedestal on outer ring deformation. This is not conducive to ensuring the working accuracy and reliability of spindle rotor system. Therefore, the outer ring fit of spindle angular contact ball bearing is usually a small clearance fit. Thermal deformation can affect the clearance fit of bearing outer ring. Under the influence of thermal deformation, the clearance fit value C can be expressed as Eq. (1).

$$C = C_0 - a_p \times \Delta T_p \times (1+\mu_p) \times d_e + a_e \times \Delta T_e \times D \,. \tag{1}$$

Where a_p and a_e are the thermal expansion coefficients of bearing pedestal and outer ring. ΔT_p and ΔT_e are the temperature rise of bearing pedestal and outer ring. C_0 is the initial clearance fit value, μ_p is Poisson's ratio of bearing pedestal and D is the diameter of bearing outer ring.

Fig. 2 shows a clearance fit diagram of bearing outer ring and pedestal. In Fig. 2, the blue grid part is the contact deformation of bearing outer ring when the bearing is loaded. δ_r is

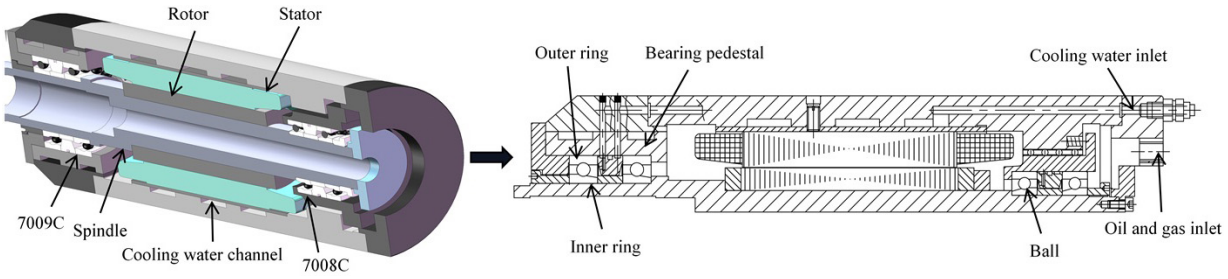

Fig. 1. Internal structure of motorized spindle.

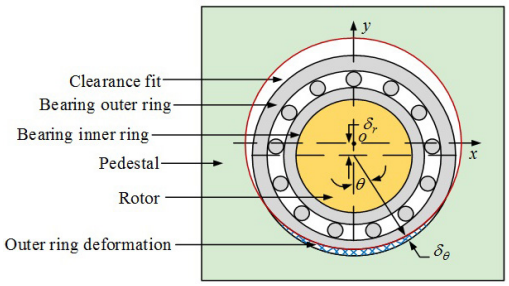

Fig. 2. Clearance fit model of bearing outer ring and pedestal.

the radial displacement of bearing outer ring. The contact deformation δ_θ at the angular position θ can be expressed as Eq. (2) [8].

$$\delta_\theta = \delta_r \cos\theta - C \,. \tag{2}$$

According to Hertz contact theory, the contact force Q_θ at the angular position θ between bearing outer ring and pedestal can expressed as Eq. (3).

$$Q_\theta = k\delta_\theta^{\frac{9}{10}} = k(\delta_r \cos\theta - C)^{\frac{9}{10}} \,. \tag{3}$$

Where k is the linear contact stiffness of material.

The contact angle range θ_{max} can be expressed as Eq. (4).

$$\theta_{\max} = 2arc\cos\frac{C}{\delta_r} \,. \tag{4}$$

By integrating the contact force in the contact area, the radial support force can be expressed as Eq. (5).

$$F_b = \int Q_\theta \cos\theta d\theta = \int_{-\frac{\theta_{\max}}{2}}^{+\frac{\theta_{\max}}{2}} k(\delta_r \cos\theta - C)^{\frac{9}{10}} \cos\theta d\theta \,. \tag{5}$$

By differentiating the ratio of the radial support force to the vibrational displacement of the outer ring, the support stiffness of the outer ring kb as affected by the clearance can be calculated.

According to the series-parallel relationship of the same type of bearing on one side inside the motorized spindle, so the outer ring support stiffness after the coupling of two bearings on the same side can be expressed as Eq. (6).

$$K_b = \frac{k_b^2}{2k_b} \,. \tag{6}$$

Fig. 3 shows the variation of radial support stiffness of the outer ring with the clearance fit value at different speeds. It can be seen that the support stiffness of the outer ring decreases with increasing speed when the clearance is not considered. In the instance of 7009C, the radial support stiffness of the outer ring drops from 161.91 kN/mm to 64.87 kN/mm as the clearance fit value increases from 0 μm to 10 μm at a speed of

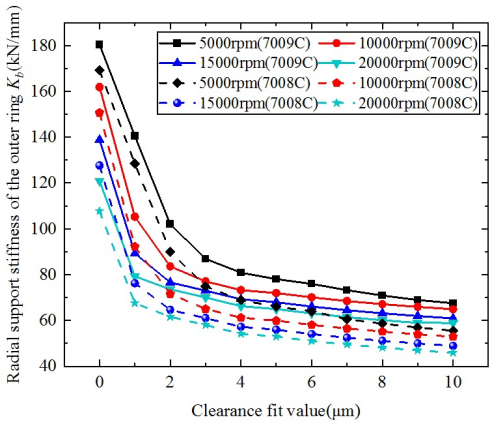

Fig. 3. Radial support stiffness of the outer ring.

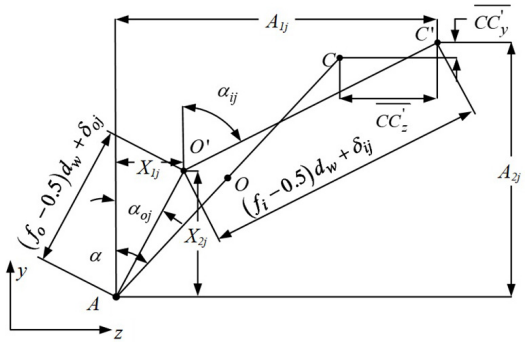

Fig. 4. Geometry relationship of curvature center and ball center.

10000 rpm. It can be concluded that as the clearance fit value increases, the support stiffness of the outer ring shows a nonlinear decrease at the same speed.

2.2 Interference fit model of bearing inner ring

The interference fit is adopted between bearing inner ring and rotor. After the bearing is installed, the curvature center of inner ring raceway groove and the contact angle change due to the effect of interference fit and preload. When the angular contact ball bearing is running, because of the bearing ball is subjected to centrifugal force, the curvature centers of the inner and outer ring raceway grooves is not on the same line as the center of the bearing ball. The curvature center of inner ring raceway groove is displaced due to the influence of centrifugal force, external load and temperature [16]. Fig. 4 shows the geometric relationship changes of bearing ball center and the curvature centers of the inner and outer ring raceway grooves. *C*, *O*, *A* are the curvature center position of inner ring raceway groove, the ball center position, and the curvature center position of outer ring raceway groove. *C'*, *O'* are the curvature center positions of inner ring raceway groove and the ball center after considering centrifugal force.

From the geometric relationship of bearing, the axial distance A_{1j} and the radial distance A_{2j} of the inner and outer ring raceway groove curvature centers can be expressed as Eq. (7) [17].

$$\begin{cases} A_{1j} = \overline{AC}\sin\alpha + \overline{CC_z'} = (f_e + f_i - 1)d_w \sin\alpha + u_a \\ A_{2j} = \overline{AC}\cos\alpha + \overline{CC_y'} \\ = (f_e + f_i - 1)d_w \cos\alpha + \delta_x \sin\psi_j + \delta_y \cos\psi_j + \Delta u \,. \end{cases} \tag{7}$$

Where f_i and f_e are the groove curvature radius coefficients of inner and outer ring raceways. δ_x and δ_y are the translational displacements of bearing inner ring. ψ_j is the angular position of the j_{th} bearing ball, R_i is the radius of bearing inner ring groove curvature center. u_a is the relative axial thermal displacement between the bearing inner and outer rings and can be expressed as Eq. (8).

$$u_a = \frac{1}{2}a_s \Delta T_s L_s - \frac{1}{2}a_p \Delta T_p L_p \,. \tag{8}$$

Where a_s is the thermal expansion coefficient of rotor, ΔT_s is the temperature rise of rotor, L_s and L_p are the axial lengths of rotor and bearing pedestal.

The relative displacement Δu between the inner and outer ring raceway groove curvature centers is caused by interference fit can be expressed as Eq. (9).

$$\Delta u = u_r + u_c + u_f \,. \tag{9}$$

Where u_r, u_c and u_f are the relative displacements between the inner and outer ring raceway groove curvature centers caused by temperature, centrifugal force and interference fit. u_r can be expressed as Eq. (10).

$$\begin{aligned} u_r = {} & a_i \times \Delta T_i \times d_i + \left[a_s \times \Delta T_s \times (1+\mu_s) - a_i \times \Delta T_i\right]\frac{d^2}{d_i} \\ & - a_p \times \Delta T_p \times (1+\mu_p) \times d_e - 2 \times a_w \times \Delta T_w \times d_w \,. \end{aligned} \tag{10}$$

Where ΔT_i is the temperature rise of bearing inner ring, a_i and a_w are the thermal expansion coefficients of bearing inner ring and bearing ball, d_i and d_e are the diameters of bearing inner and outer ring raceway grooves, d_w and d are the diameters of bearing ball and bearing inner ring.

The inner ring diameter deformation u_c under the effect of centrifugal force can be expressed as Eq. (11).

$$u_c = \frac{(1-\mu_i)d^3 + (3+\mu_i)dd_i^2}{32E_i}\rho_i \omega^2 \,. \tag{11}$$

Where μ_i is the Poisson's ratio of inner ring material, ρ_i is the material density of bearing inner ring, ω is the angular velocity of bearing inner ring, E_i is the elastic modulus of bearing inner ring.

The interference fit between bearing inner ring and rotor can cause the deformation of inner ring. Based on the elastic theory, the radial displacement of bearing inner ring can be expressed as Eq. (12) [18].

$$u_f = \frac{d \times \Delta I}{d_i} \,. \tag{12}$$

Where ΔI is the interference fit value between rotor and bearing inner ring. The interference fit of bearing inner ring makes the initial design contact angle α_0 of angular contact ball bearing change to α_1 that can be expressed as Eq. (13).

$$\cos\alpha_1 = 1 - \frac{\zeta - u_f}{2(f_e + f_i - 1)d_w} \,. \tag{13}$$

Where ζ is the design radial internal clearance. The contact angle α preload can be expressed as Eq. (14) [19].

$$\frac{F_a K^{1.5}}{N\left[(f_e + f_i - 1)d_w\right]^{1.5}} = \sin\alpha\left(\frac{\cos\alpha_1}{\cos\alpha} - 1\right)^{1.5} \,. \tag{14}$$

Where F_a is bearing preload, N is the number of balls.

The displacement equations of bearing obtained based on Pythagorean theorem in Fig. 4 can be expressed as Eq. (15).

$$\begin{cases} \left(A_{1j} - X_{1j}\right)^2 + \left(A_{2j} - X_{2j}\right)^2 - \left[(f_i - 0.5)d_w + \delta_{ij}\right]^2 = 0 \\ X_{1j}^2 + X_{2j}^2 - \left[(f_o - 0.5)d_w + \delta_{oj}\right]^2 = 0 \,. \end{cases} \tag{15}$$

Where δ_{ij} and δ_{oj} are the contact deformation of bearing ball with the inner and outer rings, X_{1j} and X_{2j} are the axial and radial distances between outer ring raceway groove curvature center and bearing ball center.

Fig. 5 shows the force analysis of bearing ball. The mechanical equilibrium equations of the bearing ball obtained by force analysis could be expressed as Eq. (16) [20].

$$\begin{cases} Q_{ij}\sin\alpha_{ij} - Q_{oj}\sin\alpha_{oj} - \dfrac{M_{gj}}{d_w}\cos\alpha_{ij} + \dfrac{M_{gj}}{d_w}\cos\alpha_{oj} = 0 \\ Q_{ij}\cos\alpha_{ij} - Q_{oj}\cos\alpha_{oj} - \dfrac{M_{gj}}{d_w}\sin\alpha_{ij} + \dfrac{M_{gj}}{d_w}\sin\alpha_{oj} + F_{cj} = 0 \,. \end{cases} \tag{16}$$

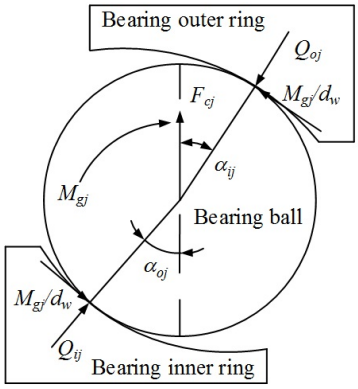

Fig. 5. Force analysis of bearing ball.

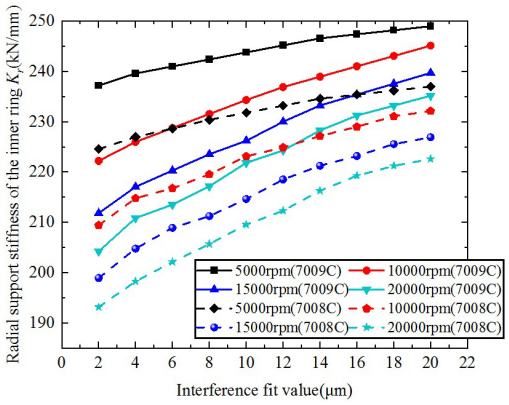

Fig. 6. Radial support stiffness of the inner ring.

Where Q_{ij} and Q_{oj} are the contact forces of bearing ball against inner and outer rings. α_{ij} and α_{oj} are the contact angels of bearing ball with inner and outer rings. M_{gj} and F_{cj} are the gyroscopic moment and centrifugal force. Simultaneous Eqs. (15) and (16) can solve variables X_{1j}, X_{2j}, δ_{ij} and δ_{oj} by Newton Raphson method. The resultant force acting on bearing inner and outer rings can be obtained by superimposing the contact force of all bearing balls. Based on the force of the inner ring, it can be deduced that the support force of the inner ring as Eq. (17).

$$\begin{cases} F_x - \sum_{i=1}^{N}\left(Q_{ij}\cdot\cos\alpha_{ij} - \dfrac{M_{gj}}{D_w}\sin\alpha_{ij}\right)\cos\psi_j = 0 \\ F_y - \sum_{i=1}^{N}\left(Q_{ij}\cdot\cos\alpha_{ij} + \dfrac{M_{gj}}{D_w}\sin\alpha_{ij}\right)\sin\psi_j = 0 . \end{cases} \tag{17}$$

Since the inner ring is rigidly connected to the rotating shaft, the radial support stiffness of the inner ring k_r affected by the interference can be obtained by differentiating the ratio of the support force to the vibration displacement of the rotating shaft [21]. According to the series-parallel relationship of the same-side bearing, the coupled inner ring support stiffness can be written as Eq. (18).

$$K_r = \frac{k_r^2}{2k_r} . \tag{18}$$

Fig. 6 gives the variation of radial support stiffness of the inner ring with the interference fit value at different speeds. It can be found that for the same interference fit value, the support stiffness decreases as the rotational speed increases. In the instance of 7009C, the radial support stiffness of the inner ring increases from 222.3 kN/mm to 245.14 kN/mm as the interference fit value increases from 2 μm to 20 μm at 10000 rpm. It can be assumed that the support stiffness of the inner ring at the same rotational speed exhibits a nonlinear rise with the increase in interference fit value.

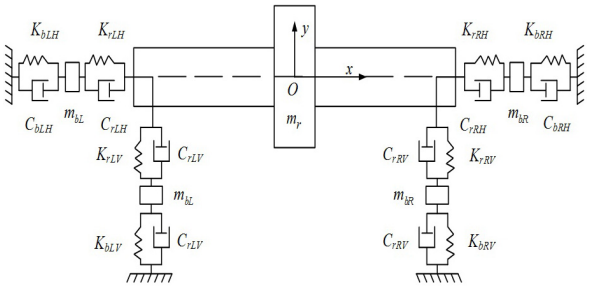

Fig. 7. Dynamic model of rotor-bearing system.

2.3 Dynamic model of rotor-bearing system

As shown in Fig. 7, the rotor-bearing system can be simplified. The rotor and bearing outer ring can be regarded as concentrated masses. In Fig. 7, O is the geometric center of rotor, and the positive direction of the y-axis is the opposite direction of gravity. The supporting effect of bearing inner ring on the rotor and the supporting effect of bearing pedestal on the bearing outer ring are regarded as two-stage spring damping systems. By solving the interference fit model of bearing inner ring and the clearance fit model of bearing outer ring, the support stiffness and damping can be obtained. According to the Newton's second law, the dynamic equation of the rotor-bearing system can be expressed as Eq. (19).

$$\begin{cases} m_r\ddot{x}_r + C_{rLH}\left(\dot{x}_r - \dot{x}_{bL}\right) + C_{rRH}\left(\dot{x}_r - \dot{x}_{bR}\right) + \\ K_{rLH}\left(x_r - x_{bL}\right) + K_{rRH}\left(x_r - x_{bR}\right) = f\omega^2\cos\left(\omega t + \varphi_0\right) \\ m_r\ddot{y}_r + C_{rLV}\left(\dot{y}_r - \dot{y}_{bL}\right) + C_{rRV}\left(\dot{y}_r - \dot{y}_{bR}\right) + \\ K_{rLV}\left(y_r - y_{bL}\right) + K_{rRV}\left(y_r - y_{bR}\right) = f\omega^2\sin\left(\omega t + \varphi_0\right) - m_r g \\ m_{bL}\ddot{x}_{bL} - C_{rLH}\left(\dot{x}_r - \dot{x}_{bL}\right) + C_{bLH}\dot{x}_{bL} - \\ K_{rLH}\left(x_r - x_{bL}\right) + K_{bLH}x_{bL} = -F_{bL}\cos\left(\omega t + \varphi_0\right) \\ m_{bL}\ddot{y}_{bL} - C_{rLV}\left(\dot{y}_r - \dot{y}_{bL}\right) + C_{bLV}\dot{y}_{bL} - \\ K_{rLV}\left(y_r - y_{bL}\right) + K_{bLV}y_{bL} = -m_{bL}\,\mathrm{g} - F_{bL}\sin\left(\omega t + \varphi_0\right) \\ m_{bR}\ddot{x}_{bR} - C_{rRH}\left(\dot{x}_r - \dot{x}_{bR}\right) + C_{bRH}\dot{x}_{bR} - \\ K_{rRH}\left(x_r - x_{bR}\right) + K_{bRH}x_{bR} = -F_{bR}\cos\left(\omega t + \varphi_0\right) \\ m_{bR}\ddot{y}_{bR} - C_{rRV}\left(\dot{y}_r - \dot{y}_{bR}\right) + C_{bRV}\dot{y}_{bR} - \\ K_{rRV}\left(y_r - y_{bR}\right) + K_{bRV}y_{bR} = -m_{bR}\,\mathrm{g} - F_{bR}\sin\left(\omega t + \varphi_0\right) . \end{cases} \tag{19}$$

Where m_r, m_{bL} and m_{bR} are the concentrated masses of the rotor, the left bearing outer ring and the right bearing outer ring, their values are m_r = 4.42 kg, m_{bL} = 0.36 kg, m_{bR} = 0.27 kg. K_{rLH}, K_{rLV}, K_{rRH} and K_{rRV} are the support stiffness of the inner ring for the left and right bearings in the horizontal and vertical directions that affected by the strength of the interference fit, K_{bLH}, K_{bLV}, K_{bRH} and K_{bRV} are the the support stiffness of the outer

ring for the left and right bearing in the horizontal and vertical directions that affected by the strength of the clearance fit. C_r, C_b are the support damping of the inner and outer ring, respectively, and they can be obtained by the equations $C_r = 0.01K_r\omega$ and $C_b = 0.25\times10^{-5}\ K_b$. x_r, x_{bL} and x_{bR} are the displacements of rotor, left and right bearing outer rings in the horizontal direction, y_r, y_{bL} and y_{bR}, respectively, are the displacements of rotor, left and right bearing outer rings in the vertical direction. f is the unbalance value, g is the gravitational acceleration.

3. Results and analysis

The dynamic equations are solved by the fourth-order Runge-Kutta method and the vibration response is analyzed. The bearings used in the simulation are 7009C and 7008C angular contact ball bearings of material GCr15, and the material selected for the rotor and bearing pedestal is 45 steel. Firstly, the temperature of spindle system at different speeds is obtained by using the thermal model of spindle system according to our previous work [13]. The stiffness of the interference fit model of bearing inner ring and the clearance fit model of bearing outer ring are calculated. In the interference fit and clearance fit models, the geometric parameters variation caused the spindle rotor-bearing system thermal displacements is considered at different speeds. Finally, the stiffness is brought into the system dynamics equation. Then the vibration response is simulated and analyzed. The simulation and calculation flow of this paper is shown in Fig. 8. The main geometric and physical parameters of the spindle rotor-bearing system are shown in Tables 1 and 2, respectively.

Table 1. Physical parameters.

Elastic modulus of bearing inner ring (E_i/Gpa)	207
Poisson's ratio of pedestal (μ_p)	0.31
Poisson's ratio of bearing inner ring (μ_i)	0.29
Thermal deformation coefficient of bearing inner ring (a_i/m·°C^{-1})	13.3e-9
Thermal deformation coefficient of bearing ball (a_w/m·°C^{-1})	13.3e-9
Thermal deformation coefficient of bearing outer ring (a_e/m·°C^{-1})	13.3e-9
Thermal deformation coefficient of rotor (a_s/m·°C^{-1})	12.5e-9
Thermal deformation coefficient of pedestal (a_p/m·°C^{-1})	12.5e-9
Bearing inner ring density (ρ_i/kg/m^3)	7810

3.1 Stability analysis

Fig. 9 reflects the variation of the system motion with the rotational speed, the interference and clearance fit values are 10 μm and 4 μm, respectively. It can be seen that the system is basically in single-period motion when the speed is below 7950 rpm, and the system vibration reaches the first peak at the speed of 7450 rpm, which indicates that this speed is the first-order critical speed. The system is in chaotic motion with multi-period characteristics at 7950~9500 rpm. With the speed

Table 2. Geometric parameters.

Property	7009C	7008C
Diameter of bearing inner ring (d/mm)	45	40
Diameter of bearing inner ring groove (d_i/mm)	54.2	48.8
Diameter of bearing outer ring groove (d_e/mm)	65.9	59.2
Diameter of bearing outer ring (D/mm)	75	68
Diameter of bearing ball (d_w/mm)	9.5	8.2
Initial contact angle (α_0/deg)	15	15
Curvature factor of inner ring raceway (f_i)	0.515	0.515
Curvature factor of outer ring raceway (f_e)	0.525	0.525
Number of balls (N)	19	19

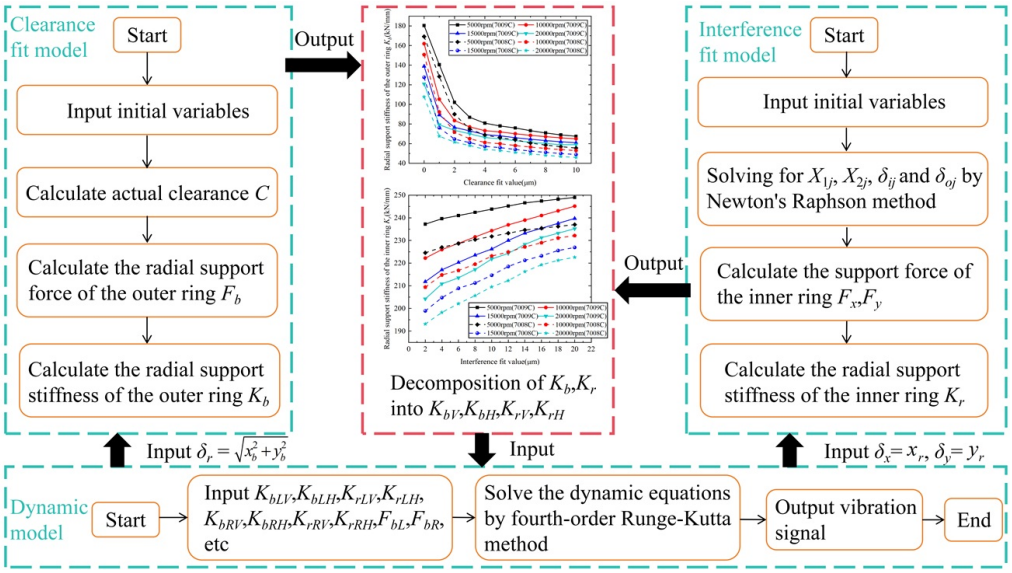

Fig. 8. Calculation flow chart.

of 9500~13500 rpm, the system changes from 4T-period motion to 2T-period motion, both of which belong to the proposed-period motion. With the increase of speed, the system finally appears chaotic motion again at 15350 rpm. The main reason is the nonlinear self-oscillation of the clearance, where the internal temperature of the bearing changes, causing the initial fit to change, resulting in dynamic changes in support stiffness and causing the system vibration to change with different kinds of periodic motion.

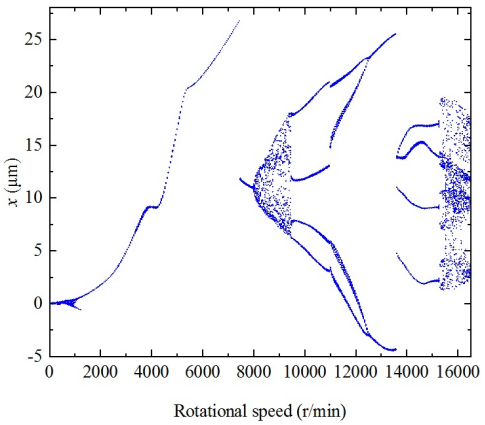

Fig. 9. Bifurcation diagram of vibration with rotational speed.

The comparison of phase trajectories and Poincare sections at the four rotational speeds is shown in Fig. 10. It can be seen that at 5000 rpm, the phase trajectory appears as an irregular circle, and only one periodic attractor appears in the Poincare section, indicating that the system is in a single-periodic motion with obvious eccentric force effect at this speed. At 9000 rpm, the phase trajectory is superimposed by many circles, which becomes more chaotic compared with Fig. 10(a), and typical chaotic attractors appear in the Poincare section, indicating that the system is in chaotic motion at this speed, and the change of clearance affects the system. At 13000 rpm, the phase trajectory takes the shape of an inner "8", and two periodic attractors appear in the Poincare section, indicating that the system is moving in 2T-period motion. When the speed reaches 15000 rpm, the phase trajectory consists of four circles, and four periodic attractors appear in the Poincare section, which means the system is in 4T-period motion. It can be considered that the speed of 9000 rpm is not conducive to the machining accuracy of the motorized spindle.

The comparison of the bifurcation diagrams for the three fits is carried out in Fig. 11. It is obvious that the motion state with 10 μm of interference fit is significantly earlier than that with 12 μm of interference fit at the same clearance fit, and the vi-

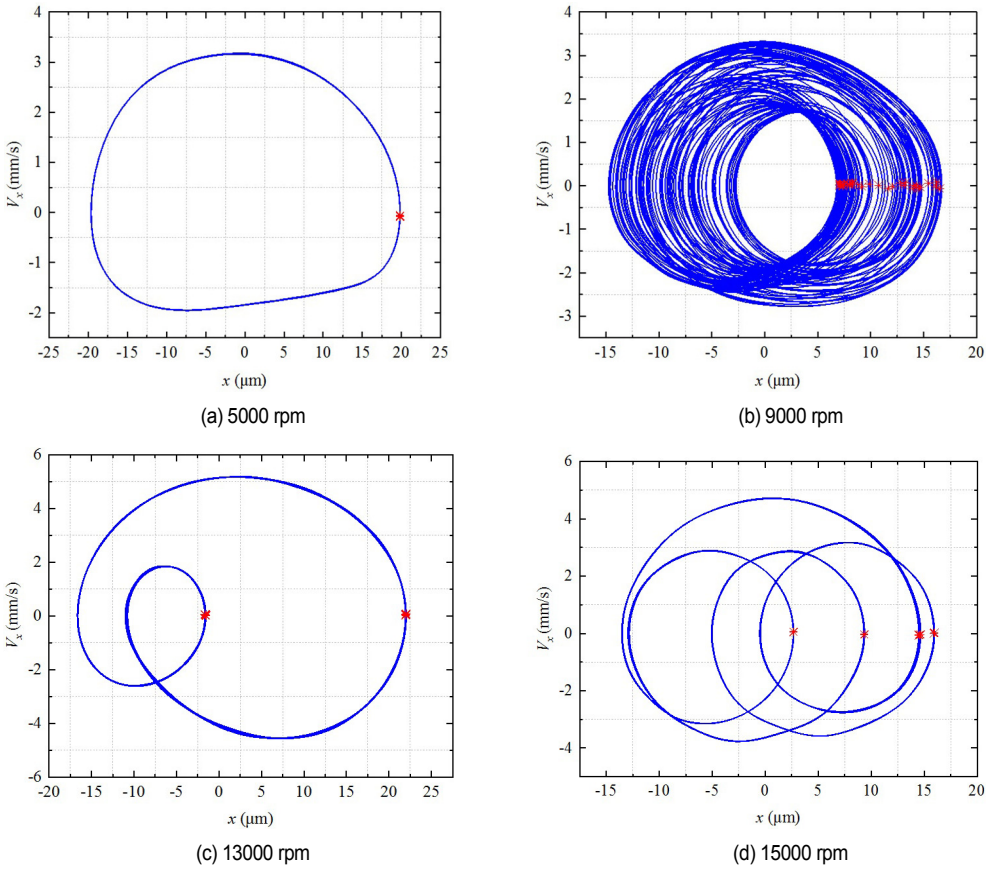

Fig. 10. Comparison of phase trajectories and Poincare sections at different rotational speeds.

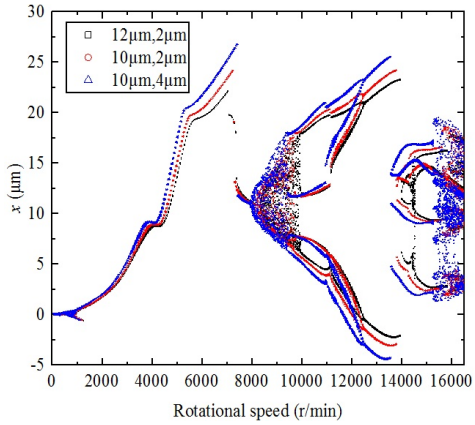

Fig. 11. Comparison of bifurcation diagrams for different fits.

bration amplitude becomes larger. Mainly due to the reduced support stiffness of inner ring caused by the reduced interference fit, the system is more affected by the nonlinear self-oscillation of clearance fit, causing the vibration amplitude of the system at the first-order critical speed to increase from 22.32 μm to 24.16 μm. The motion state with 2 μm of clearance fit, is significantly delayed compared to the motion state with 4 μm of clearance fit at the same interference fit, and the vibration amplitude becomes lower. Because of the reduced clearance fit, which causes the support stiffness of outer ring to grow, the system is less affected by the nonlinear self-oscillation of the clearance fit, resulting in the reduction of the vibration amplitude at the first-order critical speed from 26.77 μm to 24.16 μm. It can be considered that the effect of clearance fit on vibration is greater than interference fit.

3.2 Vibration analysis in time and frequency domains

Fig. 12 shows the rotor vibration displacement signals in time and frequency domains when the rotating speed is 10000 rpm, the interference and clearance fit values are 10 μm and 4 μm, respectively. It can be seen in Fig. 12(a) that the amplitude in the y-direction is obviously asymmetric due to the influence of gravity. The amplitude in the negative direction of y-direction is larger and can reach nearly 24 μm. As observed in Fig. 12(b), the rotor system generates a fundamental frequency of 166.67 Hz and a 2X frequency during operation.

Fig. 13 shows the vibration displacement signals in time domain of clearance fit values 0 μm, 4 μm, 8 μm and 12 μm. As observed in Fig. 13, the clearance fit value is larger, the vibration is greater. The vibration period also shows a longer trend. The vibration period increases as the clearance fit value. The amplitude of clearance fit value 0 μm is about 9.6 μm larger than that of clearance fit value 4 μm. The difference in amplitude of clearance fit values 4 μm and 8 μm is less than that of clearance fit values 0 μm and 4 μm. The difference in amplitude of clearance fit values 8 μm and 12 μm is also less than that of clearance fit values 0 μm and 4 μm. It shows that when

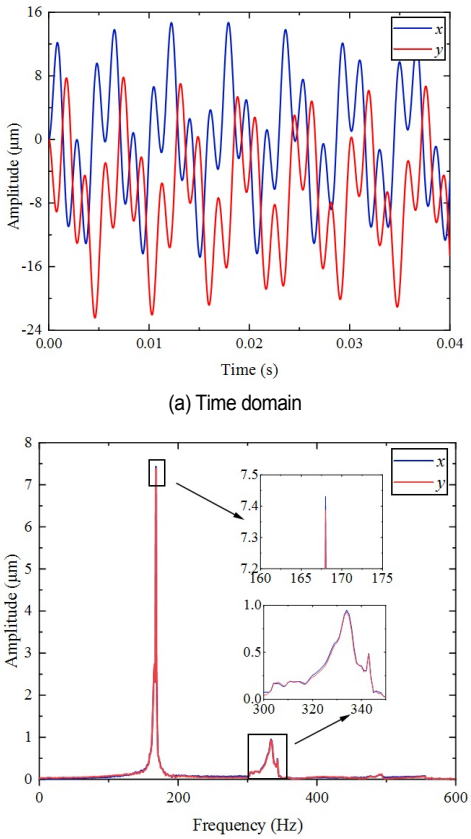

Fig. 12. The vibration displacement signals in time and frequency domains.

the clearance fit value is from 0 μm to 4 μm, it brings a big change to the vibration. As the clearance fit value becomes larger, the influence of clearance fit on the vibration relatively decreased.

Fig. 14(a) shows the spectrum with different clearance fit values when the rotating speed is 10000 rpm and the interference fit value is 10 μm. It can be seen in Fig. 14(a) that the amplitude increases as the clearance fit value. When the clearance fit value reaches 10 μm, the amplitude of 1X frequency is 7.97 μm. Fig. 14(b) is the spectrum with different interference fit values when the rotating speed is 10000 rpm and the clearance fit value is 4 μm. It can be seen in Fig. 14(a) that the amplitude decreases slightly as interference fit value. When the interference fit value reaches 18 μm, the amplitude of 1X frequency is 4.63 μm. Therefore, by comparing Figs. 14(a) with (b), it can be seen that the influence of the interference fit between bearing inner ring and rotor system on the vibration is smaller than the clearance fit, and the rotor system vibration is more sensitive to the clearance fit of bearing outer ring.

3.3 Axis trajectories analysis

In order to better compare the influence of clearance fit value and interference fit value on the axis trajectories, the rotational speed of single period motion is selected for analysis. Fig. 15

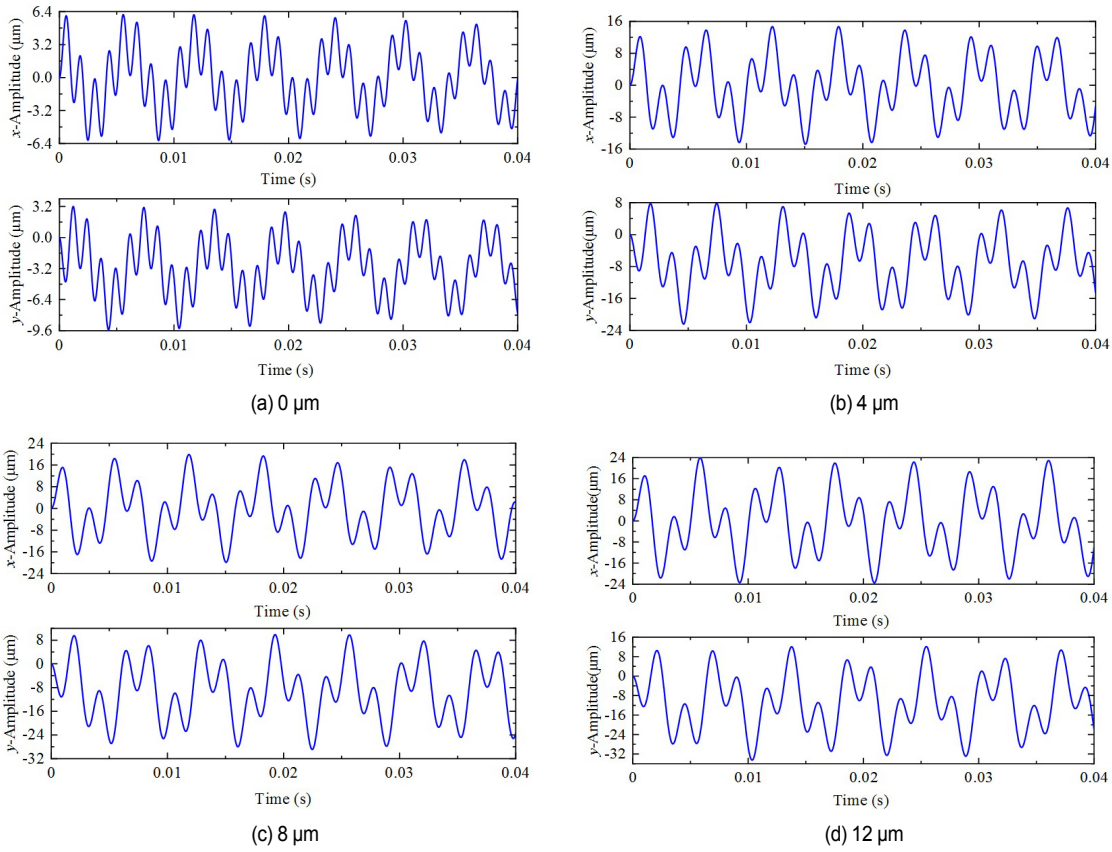

Fig. 13. The time domain diagrams with different clearance fit values.

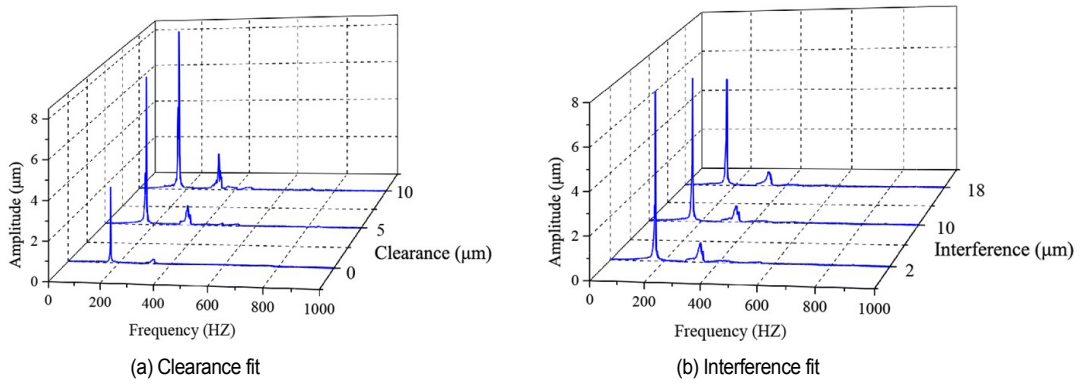

Fig. 14. The spectrum with different clearance and interference fit values.

shows the axis trajectories with different clearance fit values when rotational speed is 4000 rpm and interference fit value is 10 μm. When the clearance fit value is 0 μm, the vibration range of rotor system is about 6 μm. When the clearance fit value is 12 μm, the vibration range of rotor system is about 26 μm. With the increase of clearance fit value, the vibration range shows an obvious aggravating trend, and varies most obviously from 0 μm to 4 μm. Due to the influence of gravity, the axis trajectory is mostly in the negative direction of y-direction.

Fig. 16 presents the axis trajectories with different interfer-

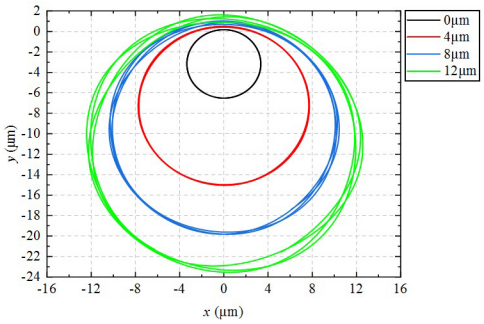

Fig. 15. The axis trajectories with different clearance fit values.

ence fit values when clearance fit value is 4 μm. When the rotational speed is 4000 rpm, the interference fit value increases from 6 μm to 18 μm, the vibration range of the axis trajectory is only reduced by 1.37 μm. It can be considered that the vibration tends to decrease slightly with the increase of interference fit value, and the interference fit value has no obvious effect on the vibration. It can be seen from the comparison with Fig. 15 that the influence of interference fit on rotor system vibration is much weaker than that of clearance fit.

3.4 Influence of the clearance and interference fit values on vibration

Fig. 17 shows the influence of interference fit value on rotor vibration with different clearance fit values when rotating speed is 4500 rpm. It can be seen in Fig. 17 that as interference fit value increases, the maximum amplitude shows a decreasing trend, and the maximum amplitude in the y-direction is larger than that in the x-direction due to the influence of gravity. The clearance fit value is 2 μm, the interference fit value is increased from 2 μm to 22 μm, and the vibration amplitude in the x-direction is decreased by 1.43 μm. The clearance fit value is 4 μm, the interference fit value is increased from 2 μm to 22 μm, and the vibration amplitude in the x-direction is decreased by 1.06 μm. It can be considered that the larger clearance fit value, interference fit value has lower influence on vibration.

The influence of clearance fit value on rotor vibration with different interference fit values is appeared in Fig. 18. It can be seen in Fig. 18 that the maximum amplitudes of different interference fit values are very close in the same direction, and the maximum amplitudes of the same interference fit values are quite different in two directions. The interference fit has little effect on vibration than gravity and clearance fit. The maximum amplitude increases nonlinearly with clearance fit values. The clearance fit value is 0 μm, the interference fit value is 4 μm, and the vibration amplitude difference of the system in x and y directions is 2.18 μm. The clearance fit value is 10 μm, the interference fit value is 4 μm, and the vibration amplitude difference between the x and y directions is 6.161 μm. It can be seen that the increase of clearance fit value has a greater influence on vibration amplitude in y-direction.

Fig. 19 shows the influence of clearance fit value on rotor vibration with unbalance values 20 g·mm and 30 g·mm when interference fit value is 10 μm. In Fig. 19, maximum amplitudes difference in two directions of unbalance value 20 g·mm is larger than that of unbalance value 30 g·mm. Increasing unbalance value can reduce the influence of gravity on vibration. It can be seen from Figs. 18 and 19, the maximum amplitude increasing trend in the x-direction has an obvious decrease

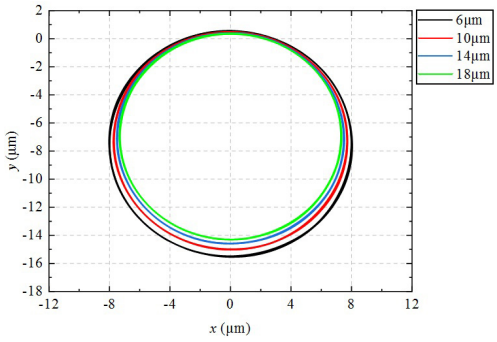

Fig. 16. The axis trajectories with different interference fit values.

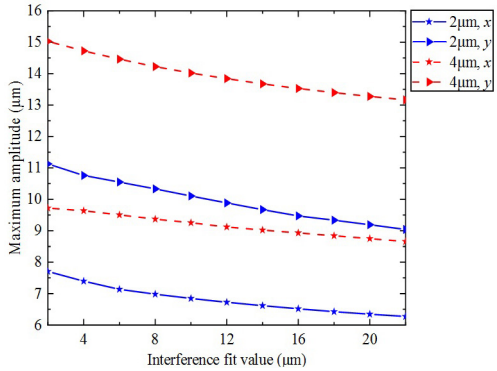

Fig. 17. Influence of interference fit value on vibration with different clearance fit values.

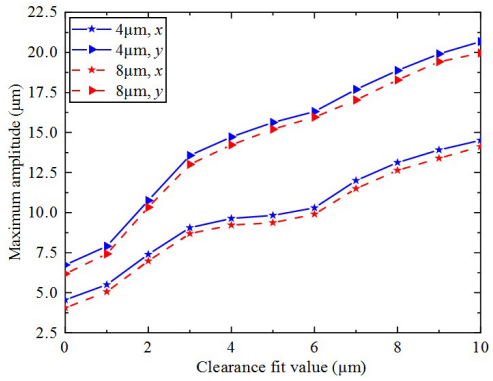

Fig. 18. Influence of clearance fit value on vibration with different interference fit values.

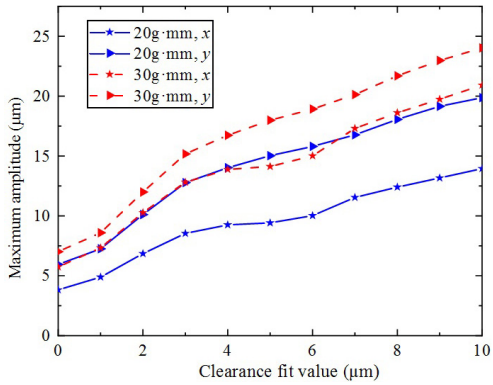

Fig. 19. Influence of clearance fit value on vibration with different unbalance values.

with clearance fit values 4 μm to 6 μm. The clearance fit value range 4 μm to 6 μm is a better choice for clearance fit between bearing outer ring and pedestal. The changes of clearance fit values in this range have the minimal influence on vibration. Although the vibration tends to be smaller at little clearance fit values, this is ignoring the effect of pedestal surface shape. In the actual situation, bearing outer ring is a precision part and the tight fit can make the shape of raceway surface tend to the shape of support surface, which can affect the running accuracy and generate noise. The decrease of the clearance fit value between bearing outer ring and pedestal also reduces the bearing internal clearance, which can affect the operation and disassembly of bearing.

4. Experimental verification

To verify the accuracy of the simulation results of the dynamics model. The experimental platform is built by using the motorized spindle(HT-170-20000-11) corresponding to the model parameters, as shown in Fig. 20. Both ends of the spindle rotor are supported by double rows of 7009C and 7008C angular contact ball bearings. The fits of front bearings 7009C are ϕ45H5/k5, ϕ75H6/h5, and the fits of rear bearings 7008C are ϕ40H6/k5, ϕ68H6/h5. The clearance fit value of bearing outer ring and the interference fit value of bearing inner ring are about 6 μm and 10 μm, respectively. The rotating speed of the motorized spindle was set to 10000 rpm. The relevant parameters of motorized spindle are shown in the Table 3.

To compare with the simulation results, other related parameters are basically consistent with the model. The preload force of the bearing is 450N. The air pressure is 0.36 Mpa. The laboratory temperature is 23 °C. Oil-air lubrication is used in the experimental process, and the flow rate is 5.5 mL/h. Cooling is carried out by water cooling, and the temperature of the cooling water is 16 °C, the flow rate is 80 mL/s.

The experiment is carried out using the laser vibrometer (OFV-505/5000 Xtra) from Polytec GmbH, Germany. The non-contact vibration measurement of the shaft end of the spindle is performed in real time by receiving the reflected signals from the laser. Then, the data collector instrument (MRBB47-01) can obtain the vibration displacement signals, and the sampling frequency can reach 100 kHz. Finally, the data display instrument (HIOKI MR8847-01) is used to export vibration data.

In order to weaken the effect of noise on the experimental results, median-averaged filtering method is used for filtering. Fig. 21 shows the time and frequency domain signals of the vibration displacement after the filtering process. From Fig. 21(a), both experimental and simulated vibration fluctuation ranges are within 30 μm. Amplitudes of experiment and simulation are broadly similar in time domain. As shown in Fig. 21(b), it is a comparison of experiment and simulation vibration dis-

Table 3. Parameters of motorized spindle.

Rotor length/mm	400
Left bearing	7009C
Right bearing	7008C
Rotating speed/(r/min)	0-20000r/min
Power/KW	11
Cooling	Liquid cooling
Lubrication	Oil-gas
Input oil/(mL/h)	5.5
Input air pressure/Mpa	0.36

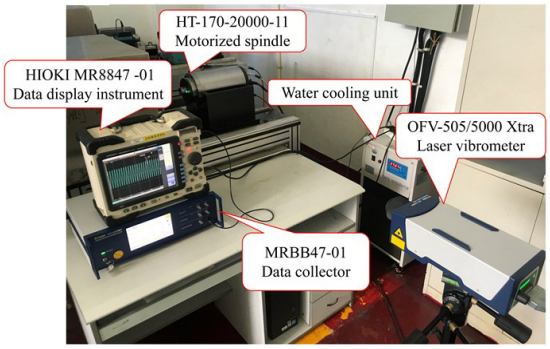

Fig. 20. Experimental test platform.

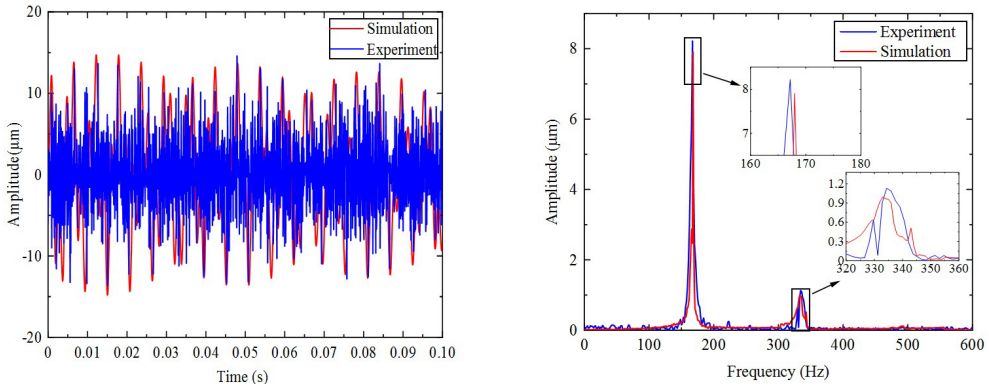

(a) Time domain (b) Frequency domain

Fig. 21. Experiment and simulation comparison of vibration.

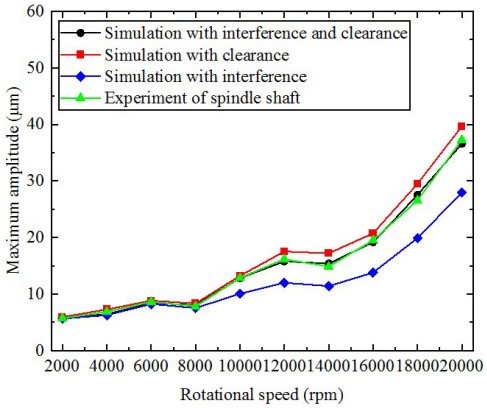

Fig. 22. Experimental and simulation comparison of vibration at different rotational speeds.

placement signals in frequency domain. Experiment and simulation both have 1X frequency and 2X frequency which are about 166 Hz and 333 Hz, respectively. The amplitudes of the experiment and simulation at 1X frequency are 8.22 μm and 7.91 μm, respectively. The amplitudes of the experiment and simulation are essentially the same.

Maximum amplitudes at different rotational speeds are measured by experiment when the clearance and interference fit values are respectively 6 μm and 10 μm. From Fig. 22, the first-order critical speed is between 6000~8000 rpm and the second-order critical speed is between 12000~14000 rpm. The simulation maximum amplitude only with clearance is the largest at 20000 rpm, its value is 39.68 μm, and the difference between it and the experiment is 2.39 μm. Only with interference, the simulation maximum amplitude is the smallest at 20000 rpm, which is 27.97 μm, and the difference between it and the experiment is 9.31 μm. The main reason is that the increase in the clearance fit value leads to the decrease in the support stiffness of the outer ring, and meanwhile, it reduces the contact range between the outer ring and the bearing pedestal, which results in the increase in the contact force and exacerbates the vibration of the system. And the increase in the interference fit value leads to therise in the support stiffness of the inner ring, which can have the effect of vibration damping. It can be considered that smaller clearance and larger interference are beneficial to reduce vibration of the system and the influence of clearance on vibration amplitude is greater than interference. With the increase of rotational speed, the maximum amplitude of vibration increases under the influence of eccentric force. The greater the rotational speed, the more obvious influence of clearance fit on vibration. The simulation results of considering bearing inner and outer ring fits are closer to the experimental results, and the maximum difference is 0.982 μm at 18000 rpm. The maximum error of simulation with experiment is 3.7 %.

5. Conclusion

In this paper, taking motorized spindle as the research object, a dynamic model of spindle rotor-bearing system considering bearing inner and outer ring fits is established. The influences of the interference fit of bearing inner ring and the clearance fit of bearing outer ring on the vibration characteristics of rotor system are mainly analyzed. The results provided are useful for the optimal design of motorized spindle system.

1) Due to the influence of clearance and interference on the support stiffness, the vibration of the system presents nonlinear characteristics such as bifurcation and reverse bifurcation with the change of rotational speed. The greater the rotational speed, the greater the influence of fit on vibration characteristics.

2) The vibration of rotor decreases with the increase of interference fit value, and increases with the increase of clearance fit value. The influence of bearing fit on vibration is nonlinear. The vibration characteristics of rotor are more sensitive to the change of clearance fit value. Compared with the interference fit of bearing inner ring, the clearance fit of bearing outer ring has a greater influence on the dynamic characteristics of system.

3) Due to the effect of bearing fit, the change of clearance fit values in range 4-6 μm has the minimal influence on rotor vibration. The maximum error of simulation considering interference and clearance fits compared with experiment is 3.7 %. A good agreement between simulation and experiment was observed.

Acknowledgments

This work was supported by the National Natural Science Foundation of China [Grant numbers: 52205117, 52175107], Exchange project of the Fourth China-Ukraine Intergovernmental Meeting [Grant numbers: 35] Key Laboratory of Vibration and Control of Aero-Propulsion System, Ministry of Education, Northeastern University [Grant No.VCAME202008], Doctor Research Project of Liaoning Provincial Science and Technology Department (Grant No. 2022-BS-193).

Nomenclature

$K_{rLH/V}$: The support stiffness of the left bearing inner ring in the horizontal/ vertical direction
$K_{bLH/V}$: The support stiffness of the left bearing outer ring in the horizontal/ vertical direction
$K_{rRH/V}$: The support stiffness of the right bearing inner ring in the horizontal/ vertical direction
$K_{bRH/V}$: The support stiffness of the right bearing outer ring in the horizontal/ vertical direction
f : The unbalance value
g : The gravitational acceleration
$C_{rLH/V}$: The support damping of the left bearing inner ring in the horizontal/vertical direction
$C_{bLH/V}$: The support damping of the left bearing outer ring in the horizontal/vertical direction
$C_{rRH/V}$: The support damping of the right bearing inner ring in the

horizontal/vertical direction
$C_{bRH/V}$: The support damping of the right bearing outer ring in the horizontal/vertical direction
μ_p : The Poisson's ratio of bearing pedestal
D : The diameter of bearing outer ring inner ring
δ_r : The radial displacement of bearing outer ring
δ_θ : The contact deformation
a_p : The thermal expansion coefficients of bearing pedestal
a_e : The thermal expansion coefficients of bearing outer ring
ΔT_p : The temperature rise of bearing pedestal
ΔT_e : The temperature rise of bearing outer ring
C_0 : The initial clearance fit
L_s : The axial lengths of rotor
L_p : The axial lengths of bearing pedestal
u_r : The relative displacements between the inner and outer ring raceway groove curvature centers caused by temperature
u_c : The relative displacements between the inner and outer ring raceway groove curvature centers caused by centrifugal force
u_f : The relative displacements between the inner and outer ring raceway groove curvature centers caused by interference fit
μ_i : The Poisson's ratio of inner ring material
ρ_i : The material density of bearing inner ring
E_i : The elastic modulus of bearing inner ring

Subscript

C : The clearance fit
I : The interference fit
b : Ball
i : Inner ring of the bearing
o : Outer ring of the bearing
αij : The contact angel of bearing ball with inner ring
α_{oj} : The contact angel of bearing ball with outer ring
Q_{ij} : The contact force of bearing ball with inner ring
Q_{oj} : The contact force of bearing ball with outer ring

References

[1] H. Cao, B. Li and Y. Li, Model-based error motion prediction and fit clearance optimization for machine tool spindles, *Mech. Syst. Signal Process*, 133 (2019) 106252.
[2] Z. Wang, Z. Wang and X. Bai, Effect of interference fit on dynamic characteristics of spindle rotor system, *J. Brazilian Soc. Mech. Sci. Eng.*, 44 (8) (2022) 316.
[3] H. Cao, F. Shi and Y. Li, Vibration and stability analysis of rotor-bearing-pedestal system due to clearance fit, *Mech. Syst. Signal Process*, 133 (2019) 106275.
[4] G. Chen and M. Qu, Modeling and analysis of fit clearance between rolling bearing outer ring and housing, *J. Sound Vib.*, 438 (2019) 419-440.
[5] H. Shi, X. Bai and K. Zhang, Effect of thermal-related fit clearance between outer ring and pedestal on the vibration of full ceramic ball bearing, *Shock Vib.*, 2019 (2019) 1-15.
[6] H. Shi, Y. Li and X. Bai, Investigation of the orbit-spinning behaviors of the outer ring in a full ceramic ball bearing-steel pedestal system in wide temperature ranges, *Mech. Syst. Signal Process*, 149 (2021) 107317.
[7] D. Wu, Q. Han and H. Wang, Nonlinear dynamic analysis of rotor-bearing-pedestal systems with multiple fit clearances, *IEEE Access*, 8 (2020) 26715-26725.
[8] D. Zhang, D. Wu and Q. Han, Dynamic force transmissibility of flywheel rotor systems supported by angular contact ball bearings considering clearance fit, *Eur. J. Mech. A/Solids*, 92 (2022) 104457.
[9] Y. Mao, L. Wang and C. Zhang, Influence of ring deformation on the dynamic characteristics of a roller bearing in clearance fit with housing, *Int. J. Mech. Sci.*, 138 (2018) 122-130.
[10] X. Li, Y. Lv and K. Yan, Study on the influence of thermal characteristics of rolling bearings and spindle resulted in condition of improper assembly, *Appl. Therm. Eng.*, 114 (2017) 221-233.
[11] H. Wang, Passive vibration reduction of a squeeze film damper for a rotor system with fit looseness between outer ring and housing, *J. Low Freq. Noise Vib. Act. Control.*, 40 (3) (2021) 1473-1492.
[12] K. Feng, J. Wang and Y. Zuo, Simulation analysis method for equivalent mechanical characteristics of rotor asymmetric supports with bearing clearance, *Journal of Mechanical Engineering*, 57 (19) (2021) 138-146.
[13] Z. Wang, K. Zhang and Z. Wang, Research on vibration of ceramic motorized spindle influenced by interference and thermal displacement, *J. Mech. Sci. Technol.*, 35 (6) (2021) 2325-2335.
[14] T. Guo, X. Ma and Y. Gu, Effect of the interference fit amount impact on the dynamic characteristics of spindle, *Journal of Beijing University of Technology*, 42 (2016) 51-59.
[15] G. Liu, J. Hong and W. Wu, Investigation on the influence of interference fit on the static and dynamic characteristics of spindle system, *Int. J. Adv. Manuf. Technol.*, 99 (2018) 1953-1966.
[16] M. Alfares, O. Saleem and M. Majeed, Analytical study of thermal variation impact on dynamics of a spindle bearing system, *Proc. IMechE, Part K: J. Multi-body Dynamics*, 233 (4) (2019) 871-898.
[17] X. Zhang, Q. Han and Z. Peng, Stability analysis of a rotor-bearing system with time-varying bearing stiffness due to finite number of balls and unbalanced force, *J. Sound Vib.*, 332 (25) (2013) 6768-6784.
[18] T. A. Harris and M. N. Kotzalas, *Rolling Bearing Analysis: Essential Concepts of Bearing Technology*, Taylor and Francis, USA (2007).
[19] K. Xu, B. Wang and Z. Zhao, The influence of rolling bearing parameters on the nonlinear dynamic response and cutting stability of high-speed spindle systems, *Mech. Syst. Signal Process*, 136 (2020) 106448.
[20] X. Li, K. Yu and H. Ma, Analysis of varying contact angles and load distributions in defective angular contact ball bearing, *Eng. Fail Anal*, 91 (2018) 449-464.
[21] Y. Liu and Y. Zhang, A research on the time-varying stiffness

of the ball bearing considering the time-varying number of laden balls and load distribution, *Proc. IMechE, Part C: J. Mechanical Engineering Science*, 233 (12) (2019) 4381-4396.

Zhan Wang is a Professor of School of Mechanical Engineering, Shenyang Jianzhu University, Shenyang, China. He received his Ph.D. in Mechanical Design and Theory from Northeastern University, China. His research interests include dynamics and vibration control of the spindle.

Zinan Wang is an Associate Professor in the School of Mechanical Engineering, Shenyang Jianzhu University, Shenyang, China. His research work is focused on the dynamic characteristics analysis of spindle rotor system.